Biophysical Chemistry 151 (2010) 139–148

Contents lists available at ScienceDirect

Biophysical Chemistry

journal homepage: http://www.elsevier.com/locate/biophyschem

NMR studies of new arginine vasopressin analogs modified with α-2-indanylglycine enantiomers at position 2 bound to sodium dodecyl sulfate micelles

Emilia Lubecka, Anna Kwiatkowska, Jerzy Ciarkowski, Emilia Sikorska *

Faculty of Chemistry, University of Gdańsk, Sobieskiego 18, 80-952 Gdańsk, Poland

ARTICLE INFO

Article history:
Received 28 April 2010
Received in revised form 8 June 2010
Accepted 8 June 2010
Available online 16 June 2010

Keywords:
α-2-Indanylglycine
Vasopressin
SDS micelle
NMR spectroscopy
Molecular modeling

ABSTRACT

In this paper, we use NMR spectroscopy and molecular modeling to examine four new vasopressin analogs modified with α-2-indanylglycine (Igl) at position 2, [L-Igl^2]AVP (**I**), [D-Igl^2]AVP (**II**), [Mpa^1,L-Igl^2]AVP (**III**) and [Mpa^1,D-Igl^2]AVP (**IV**), embedded in a sodium dodecyl sulfate (SDS) micelle. All the analogs display antiuterotonic activity. In addition, the analogs with D-Igl reveal antipressor properties.
Each analog exhibits the tendency to adopt β-turns at positions 2, 3 and/or 3, 4, which is characteristic of oxytocin-like peptides. Mutual arrangement of aromatic residues at positions 2 and 3 has been found to be crucial for binding antagonists with the OT and V_{1a} receptors. The orientation of the Gln^4 side chain seems to be important for the V_{1a} receptor affinity. In each of the peptides studied, the Gln^4 side chain is folded back over the ring moiety. However, it lies on the opposite face of the tocin moiety in analogs with L and D enantiomers of Igl.

1. Introduction

Arginine vasopressin (AVP), a neurohypophyseal hormone and a neuromodulator, is a nonapeptide with a disulfide bridge between Cys residues at positions 1 and 6. It plays a very important role in controlling resorption of water by the distal tubules of the kidney and regulating the osmotic pressure of blood [1,2]. Besides, AVP is responsible for stimulation of the adrenocorticotropine secretion [3] and stability of the body temperature [4]. It exhibits also oxytocic activity [5]. Moreover, recent studies have shown that vasopressin, together with oxytocin, might also take part in autism and provide an effective treatment of autism's repetitive and affiliative behaviors [6,7].

The biological effects of vasopressin are mediated by four different receptor subtypes: V_2 (renal), V_{1a} (vasopressor), V_{1b} (pituitary) and OT (uterine), being typical members of class A GPCR, which are membrane-spanning proteins [8]. The current model for peptide hormone interactions with their receptors suggests that the bioactive conformation of the peptide is induced upon association with the cell membrane followed by a two-dimensional diffusion process, whereby the peptide is recognized and then interacts with the receptor [9,10]. Therefore, exploring the conformational and dynamic properties of a ligand in a membrane-mimicking environment can contribute to better understanding of the molecular features involved in their interactions with the target receptor.

It is believed that the tyrosine residue at position 2 of AVP plays a part initiating the pressor response of AVP [11]. The substitution of Tyr with its D enantiomer produces an analog with only partial agonist activity, whereas the deletion or O-alkylation of Tyr^2 hydroxyl group results in antagonistic properties [12]. Similarly, replacement of Tyr^2 of AVP with bulky or sterically restricted substituents is generally favorable for generation of effective antagonists [13,14].

In this paper, we use NMR spectroscopy and molecular modeling to examine four new vasopressin analogs modified with α-2-indanylglycine (Igl) (Fig. 1) at position 2, [L-Igl^2]AVP (**I**), [D-Igl^2]AVP (**II**), [Mpa^1,L-Igl^2]AVP (**III**) and [Mpa^1,D-Igl^2]AVP (**IV**) embedded in a sodium dodecyl sulfate (SDS) micelle. Although, dodecyphosphocholine (DPC) provides a zwitterionic surface on the micelle that better mimics the biological membranes of the vertebrates, we decided to use the SDS micelle with negatively charged head groups, because the AVP analogs modified with Igl are poorly soluble positively charged peptides, which advises towards incorporation of net negative charges on the SDS micelle surface in order to improve peptide/micelle solubility [15].

The α-indanylglycine was earlier successfully applied for the synthesis of potent and totally enzyme-resistant bradykinin antagonists [16]. In turn, the deamination of cysteine at position 1, usually enhances antidiuretic activity and V_2/V_{1a} selectivity [17]. However, most of oxytocin antagonists describe to date contain Mpa (Fig. 1) instead of Cys^1 [18].

All the studied analogs exhibit only negligible antidiuretic activity. The [L-Igl^2]AVP (**I**) and [Mpa^1,L-Igl^2]AVP (**III**) analogs are moderately potent but selective OTR antagonists. In turn, those modified with enantiomer D of Igl have dual activity—they show high antioxytocic potency at low and full oxytocic agonism at high concentrations [19]. This phenomenon is difficult to explain. However, similar effect has been reported for

Abbreviations: AVP, arginine vasopressin; GPCR, G-protein coupled receptor; Igl, α-2-indanylglycine; Mpa, 3-mercaptopropionic acid; OT, oxytocin; SDS, sodium dodecyl sulfate.

* Corresponding author.
E-mail address: milka@chem.univ.gda.pl (E. Sikorska).

0301-4622/$ – see front matter © 2010 Elsevier B.V. All rights reserved.
doi:10.1016/j.bpc.2010.06.002

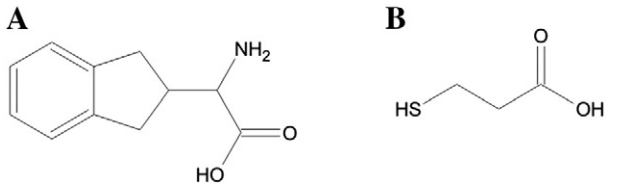

Fig. 1. (A) 2-α-Indanylglycine (Igl) and (B) 3-mercaptopropionic acid (Mpa).

naloxone, an opioid antagonist at low concentration and partial agonist at a high one. The changeover of the activity of naloxone from antagonistic to agonistic is probably the result of a slight desensitization and down regulation of the opioid receptors [20].

2. Materials and methods

2.1. Peptide synthesis and purification

The peptides were synthesized using the standard 9-fluorenylmetoxycarbonyl (Fmoc) methodology (full details including protecting groups, deprotection and cyclication have been reported recently [19]). After HPLC purification, their purity was higher than 98% as determined by analytical HPLC. The MALDI TOF mass spectrometry confirmed that the purified peptides were the desired products.

2.2. Sample preparation

The SDS-d_{25} was purchased from Sigma Aldrich. The samples in the SDS micelle were prepared at a concentration of about 3 mM of a peptide in 0.7 ml of a partially deuterated phosphate buffer (90% H_2O and 10% D_2O) of pH = 7.4 containing about 35 mg of SDS-d_{25}. The SDS-d_{25}:peptide ratio was adjusted to approximately 1:40. The SDS-d_{25} concentration exceeded considerably the critical micelle concentration of SDS (8.3 mM), to be sure that the peptides were indeed micelle-bound.

2.3. NMR measurements

All the NMR experiments were recorded on a 500 MHz Varian spectrometer equipped with a Performa II gradient generator unit, WFG, Ultrashims, a high stability temperature unit and a 5 mm $^1H\{^{13}C/^{15}N\}$

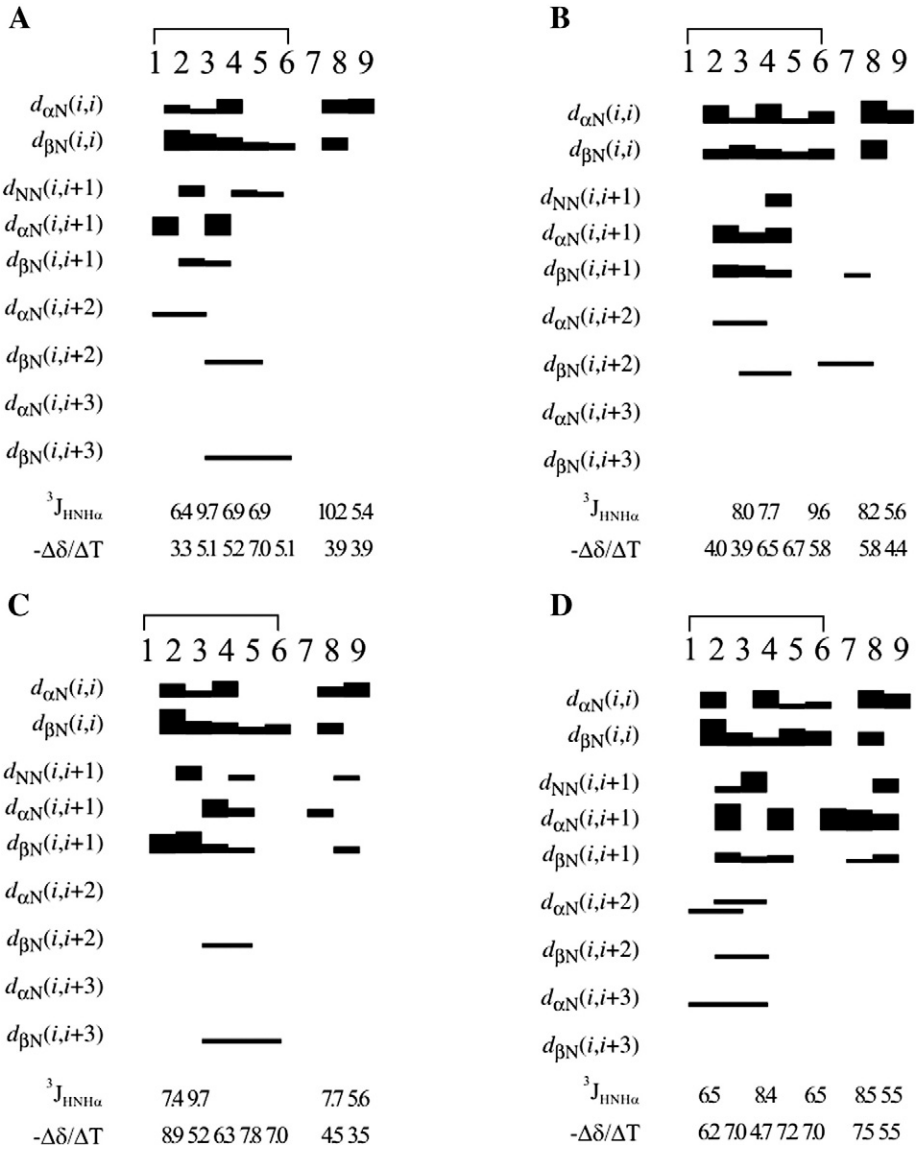

Fig. 2. The NOE effects corresponding to the interproton distances, $^3J_{HNH\alpha}$ coupling constants and the temperature coefficients of the backbone amide atoms of (A) [L-Igl^2]AVP (**I**), (B) [D-Igl^2]AVP (**II**), (C) [Mpa^1,L-Igl^2]AVP (**III**) and (D) [Mpa^1,D-Igl^2]AVP (**IV**).

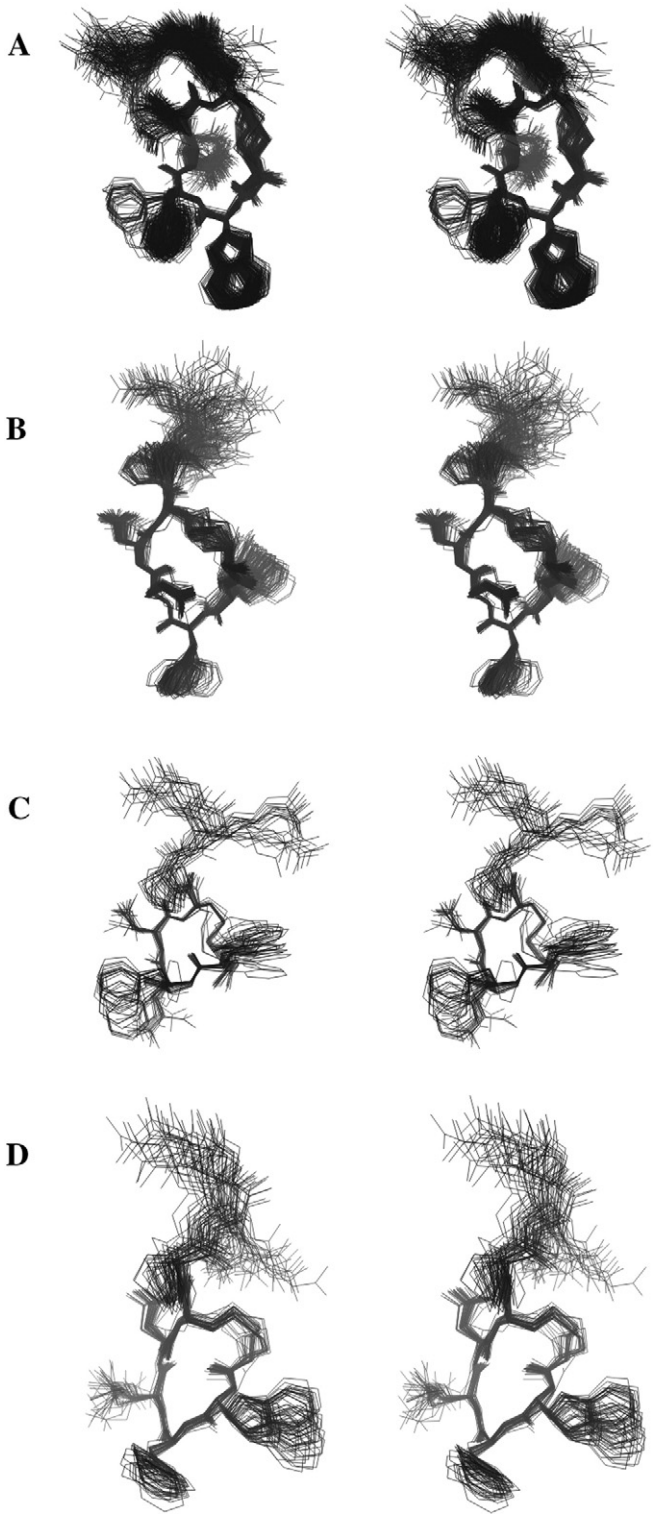

Fig. 3. Stereoview showing the conformational ensembles of (A) [L-Igl^2]AVP (**I**), (B) [D-zIgl^2]AVP (**II**), (C) [Mpa^1,L-Igl^2]AVP (**III**) and (D) [Mpa^1,D-Igl^2]AVP (**IV**) obtained by fitting the statistical weights of MD-generated conformations. RMSD = 0.288, 0.276, 0.226 and 0.195 for backbone atoms of cyclic part, respectively.

PFG triple resonance inverse probe head (Intercollegiate NMR Laboratory, Faculty of Chemistry, Gdansk University of Technology, Poland).

The 2D NMR spectra were taken at 30 °C. The temperature coefficients of the amide proton chemical shifts were measured from 1D NMR spectra at 22, 25, 30, 35, 40, 45 and 50 °C. Proton resonance assignments were achieved by use of the proton–proton total chemical shift correlation spectroscopy (TOCSY) [21], double quantum filtered correlation spectroscopy (DQF-COSY) [22], the nuclear Overhauser effect spectroscopy (NOESY) [23], the rotating-frame Overhauser enhancement spectroscopy (ROESY) [24,25], as well as the gradient heteronuclear single quantum coherence (^{1}H–^{13}C gHSQC) [26–28]. All the spectra were measured with a water signal pre-saturation pulse typically of 2 dB and 1.5 s. In the case of the 1D NMR spectra, 16 K data points were collected and a spectral width of 8 kHz was used. The homonuclear TOCSY (80 ms), NOESY (200 ms), ROESY (200 and 300 ms) and DQF-COSY were recorded in the range of 0.5–9.5 ppm, with 32–64 scans per t_1, a spectral width of 4.5 kHz in both dimensions, and 512 × 2 K data sets, which were then zero-filled to 1 K × 2 K after Fourier transform. Data size for ^{1}H–^{13}C HSQC spectrum was 256 (t_1)–1024 (t_2) and spectral widths were 18 kHz in the ^{13}C dimension and 4.5 kHz in the ^{1}H dimension. For this experiment, a total number of 128 transients were used.

Vicinal coupling constants, $^3J_{HNH\alpha}$, were assigned using DQF-COSY and 1D NMR spectra. The DQF-COSY spectra were processed to enhance the resolution to 1.2 Hz per point in F2. For Gly residues, the two $^3J_{HNH\alpha}$ coupling constants are equal within the limits of error.

The proton chemical shifts were referenced to the H_2O frequency measured with respect to external 2,2-dimethyl-2-silapentanesulfonic acid (DSS). The ^{13}C chemical shifts were referenced to DSS according to the following relationship: $^{13}C/^1H = 0.251449530$ [29]. The data were processed using VNMR 6.1B (Varian Inc., Palo Alto, CA) and the spectra were analyzed using XEASY [30].

2.4. Molecular modeling

The calculations consisted of the following three steps: (*i*) search of the conformational space by employing molecular dynamics simulations, (*ii*) simulation of the NOE spectrum and vicinal coupling constants for each conformation, and (*iii*) determination of the statistical weights of the conformations to obtain the best fit of the averaged NOE intensities and coupling constants to the experimental quantities [31].

Molecular dynamics simulations were carried out with the AMBER force field [32]. The valence geometries of the residues not specified in the standard AMBER database, were parameterized as recommended by the AMBER 9.0 manual [32]. Specifically, these residues were modeled using bond lengths, the valence and torsion angles of appropriate residues and compatible molecular segments taken from the CSDS [33] database. The point charges were optimized by fitting them to the *ab initio* molecular electrostatic potential (6-31G* basis set, GAMESS'04 [34]—*ab initio* molecular electronic structure program) for two different conformations of every non-standard residue, followed by consecutive averaging the charges over all conformations, as recommended by the RESP protocol [35].

The preparation of the micelle was initiated by construction of a single molecule of sodium dodecyl sulfate (SDS) based on the literature parameters [36,37]. The entire procedure has been described by us previously [38]. Initial structures of the peptides were generated in random conformation. The peptide groups were kept fixed to trans geometry with force constant f = 50 kcal/(mol × rad^2) during the entire simulations. The calculations were performed only for major conformations. Each peptide was placed in a simulation box with its centre of mass coinciding with that of the micelle. Owing to the spherical symmetry of the micelle, the orientation of the peptide was unimportant. The side chain of Arg^8 and the N-terminus were protonated. Thus, the [Igl^2]AVP (**I**) and [D-Igl^2]AVP (**II**) had a total charge of +2, while the total charge of [Mpa^1,Igl^2]AVP (**III**) and [Mpa^1,D-Igl^2]AVP (**IV**) was equal to +1. To neutralize the entire system, chloride ions were added.

To eliminate initial bad contacts between a peptide and the micelle core, and to prevent penetration of water during equilibration, the peptide and the bulk water were kept under weak harmonic constraints with force constants of 10 and 5 kcal/(mol×Å), respectively. These

Table 1
Structural statistics for the set of the conformations of [Igl^2]AVP (**I**), [D-Igl^2]AVP (**II**), [Mpa^1,Igl^2]AVP (**III**) and [Mpa^1,D-Igl^2]AVP (**IV**) constituting 60% of the ensemble.

Statistic	Peptide							
	I		**II**		**III**		**IV**	
NOE connectivities								
Intraresidual	56		60		65		75	
Sequential	14		19		23		28	
Medium-range	5		4		7		12	
Long-range	0		0		1		0	
Sd in peak volume	1.4		0.6		0.9		2.9	
$^3J_{HNH\alpha}$	J_{exp}	J_{calc}	J_{exp}	J_{calc}	J_{exp}	J_{calc}	J_{exp}	J_{calc}
Cys^1/Mpa^1	n.o.	n.o.	n.o.	n.o.	–	–	–	–
L-Igl^2/D-Igl^2	6.4	6.6	n.o.	n.o.	7.4	5.9	6.5	5.0
Phe^3	9.7	9.4	8.0	8.9	9.7	9.4	n.o.	n.o.
Gln^4	6.9	7.7	7.7	8.4	n.o.	n.o.	8.4	7.9
Asn^5	6.9	6.6	n.o.	n.o.	n.o.	n.o.	n.o.	n.o.
Cys^6	n.o.	n.o.	9.6	9.0	n.o.	n.o.	6.5	7.8
Pro^7	–	–	–	–	–	–	–	–
Arg^8	10.2	10.3	8.2	7.9	7.7	8.2	8.5	8.8
Gly^9	5.4	5.2	5.6	5.2	5.6	5.1	5.7	5.3
Sd in coupling constant	0.4		0.7		0.9		1.0	
The numbers of conformations constituting 60% of the ensemble	194		111		23		42	
Atomic r.m.s. differences (Å)								
Backbone atoms 1–6	0.288		0.276		0.226		0.195	
Heavy atoms 1–6	0.908		0.680		0.786		0.746	
Conformational properties								
Reverse structures	2,3 βI 6,7 βI or III 7,8 βI or IV		2,3 βI or IV 3,4 βI or IV		2,3 βII 3,4 βIII' 4,5 β I' or II' 7 γ*		2,3 βII' 3,4 βI	
Hydrogen bonds	HN^4–CO^1 HN^8–CO^5 HN^9–CO^5 s.c.^{8}–s.c.^{5}		HN^{2,3}–εCO^4		HN^4–CO^1 HN^{5,6}–CO^2 HN^8–CO^6		s.c.^{8}–s.c.^{5}	
Radius of gyration (Å)								
Heavy atoms	6.3		7.1		6.2		6.4	
Heavy atoms 1–6	5.3		5.3		4.9		5.0	

SD—standard deviation.
n.o.—not observed.
s.c.—side chain.

constraints were removed in 20,000 steps of minimization (steepest descent method). The entire system was then minimized for 20,000 steps. Thereafter, the system was equilibrated under a constant pressure at 303 K for 2 ns. Afterwards, the LES (locally enhanced sampling) [39] system was used. This technique allows selective application of additional computational effort to a portion of the system, thus increasing the sampling of the region of interest. The enhanced sampling is achieved by replacing the region of interest with multiple copies. During the simulation, the copies are free to move apart and explore different regions of conformational space, thereby increasing the statistical sampling. A total of three copies of each peptide were generated by ADDLES module of the AMBER 9.0 program. During MD simulation, a 9 Å cut-off radius was chosen. The MD simulations were carried out at 303 K in a periodic box of constant volume, with the Particle-mesh Ewald (PME) procedure. The time step was 2 fs. The total duration of the LES run was 4 ns. The coordinates were collected every 2000th step. The conformations obtained during the last 800 ps of simulation were considered in further analysis. As a result, the set of 600 conformations for each peptide was obtained.

Next, the theoretical NOE spectrum and $^3J_{HNH\alpha}$ vicinal coupling constants were calculated using the MORASS [40] program for each conformation. This program solves the system of Bloch differential equations for the cross-relaxation of a system of interacting proton spins. The vicinal couplings, $^3J_{HNH\alpha}$, were calculated from the empirical Bystrov–Karplus relationship [41]. The NOE effects were generated using a correlation time of 0.45 ns [42], mixing time of 200 ms and a cut-off value of 6 Å. The weight of the coupling-constant term was 0.2. The populations of the conformations, described by statistical weights, were determined by fitting a linear combination of the generated spectra and coupling constants to the experimental data with an entropy factor, $\alpha = 0.2$ [31]. To describe the structural preference of each peptide we used the structures constituting about 60% of the ensemble obtained from calculations. As a result 194, 111, 24 and 42 conformations of analogs **I**, **II**, **III** and **IV**, respectively, were considered.

The results were analyzed using the Carnal and Ptraj programs from the AMBER 9.0 package [32]. To find the peptide–micelle interactions, the radial distribution functions (RDFs) between the side chains and negatively charged groups of the SDS micelle and also between the side chains and the micelle core atoms were calculated. The data were averaged over the conformations with the sum of their statistical weights amounting to 60%. To estimate the interactions between the peptides and aqueous environment, hydration numbers were also calculated, as a method of quantifying the interactions between the peptides and water. The hydration number is an integral radial distribution function showing how many water molecules are located near the residue. Two sets of the hydration numbers were calculated for each system, one for the side chains heavy atoms, and the other for the carbonyl oxygen for each residue for a hydration radius of 3.8 Å.

The molecular structures were drawn and analyzed with the MOLMOL [43] graphic program.

3. Results and discussion

3.1. Analysis of the NMR spectra

The NMR spectra of analog **II** and **IV** indicate that the Phe^3, Gln^4, Asn^5, and Arg^8 residues are at equilibrium between two conformational states. In analog **IV**, two distinct sets of residual proton resonances were

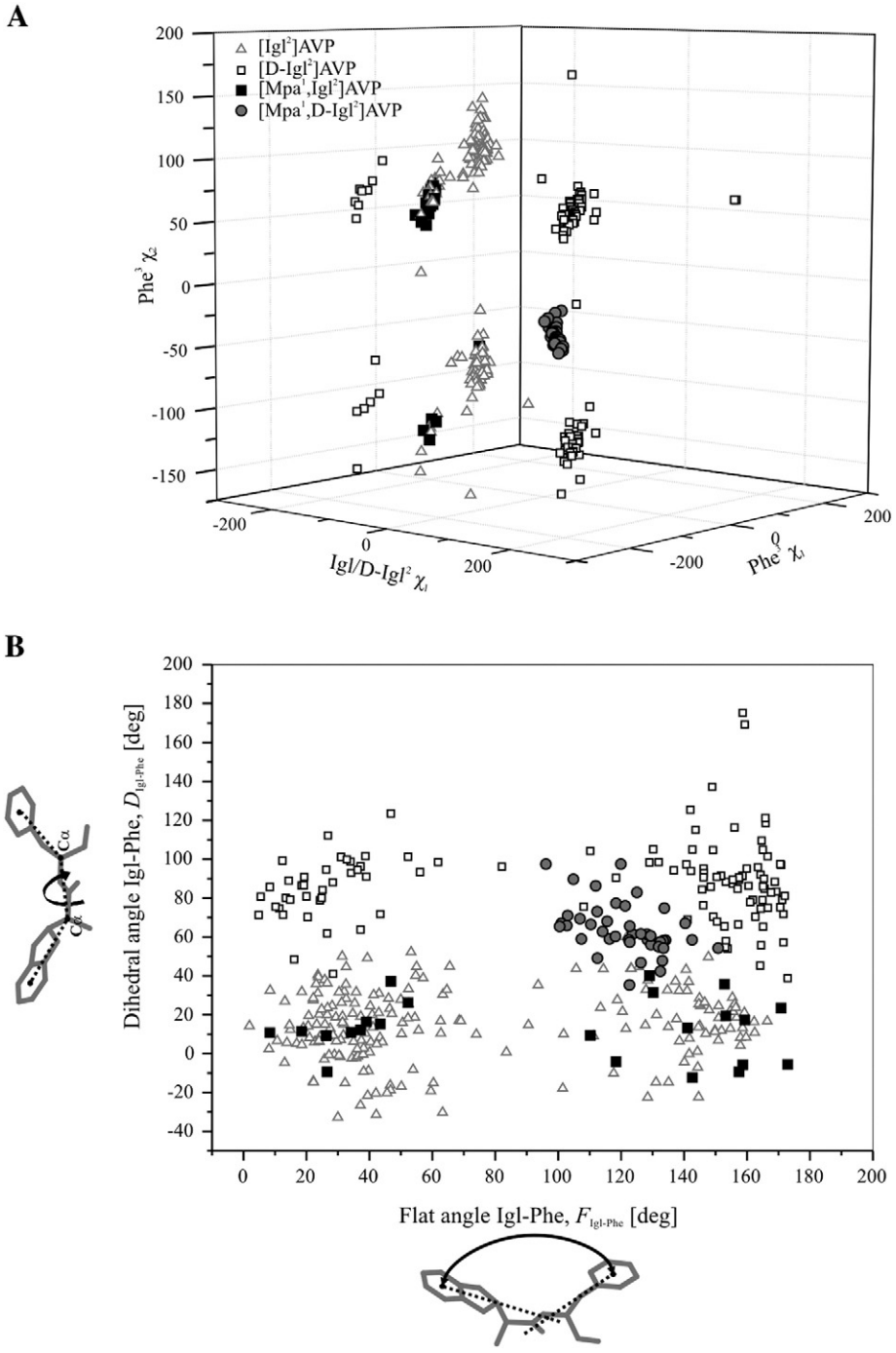

Fig. 4. (A) Scatter plots of the side chain dihedral angles (χ_1:N-Cα-Cβ-Cγ1 of Igl/D-Igl^2, χ_1:N-Cα-Cβ-Cγ and χ_2:Cα-Cβ-Cγ-Cδ1 of Phe^3) of aromatic residues of [L-Igl^2]AVP (**I**), [D-Igl^2]AVP (**II**), [Mpa^1,L-Igl^2]AVP (**III**) and [Mpa^1,D-Igl^2]AVP (**IV**) and (B) the relationship between the flat angle between the planes of aromatic rings ($F_{\text{Igl-Phe}}$) and dihedral angle between two planes, where the former is determined by the centre of mass of aromatic part of Igl/D-Igl^2, Cα of Igl/D-Igl^2 and Cα of Phe^3, whereas the latter by Cα of Igl/D-Igl^2, Cα of Phe^3 and the centre of mass of aromatic ring of Phe^3 ($D_{\text{Igl-Phe}}$).

also found for Gly^9. The intensity ratio of both conformers is equal approximately to 5.6:1 for each peptide. On the other hand, only one set of the chemical shifts was found for the remaining residues. The appearance of two conformers is likely to be due to either the *cis*/*trans* isomerization of the Cys^6–Pro^7 peptide bond or different interactions of the peptides with the SDS micelle. The former hypothesis could be verified by an exchange *trans*Hα(Pro)–*cis*Hα(Pro) cross-peak and/or cisHα(Cys)–cisHα(Pro) connectivity. However, they were not found in the ROESY and/or NOESY spectra. In turn, taking into account the latter hypothesis, strong electrostatic interactions between the positively charged Arg^8 side chain and the negatively charged sulfate groups at the micelle surface could be expected. Hence, the Arg^8 should be strongly bound to the micelle surface and a smaller conformational space should be accessible than for the remaining residues. Consequently, only one set of proton resonance for Arg is likely to exist. Therefore, we cannot validate the origin of the two conformers unambiguously. The proton chemical shifts of the peptides are summarized in Tables S1 and S2 (Supplementary materials).

It is known that the sequential $d_{NN}(i,i+1)$ NOE connectivities are seen only in those regions of peptides which preferentially adopt folded conformations [44]. Therefore, the scrutiny of the NOE patterns (Fig. 2) suggests that all the analogs adopt primarily reverse structures in their

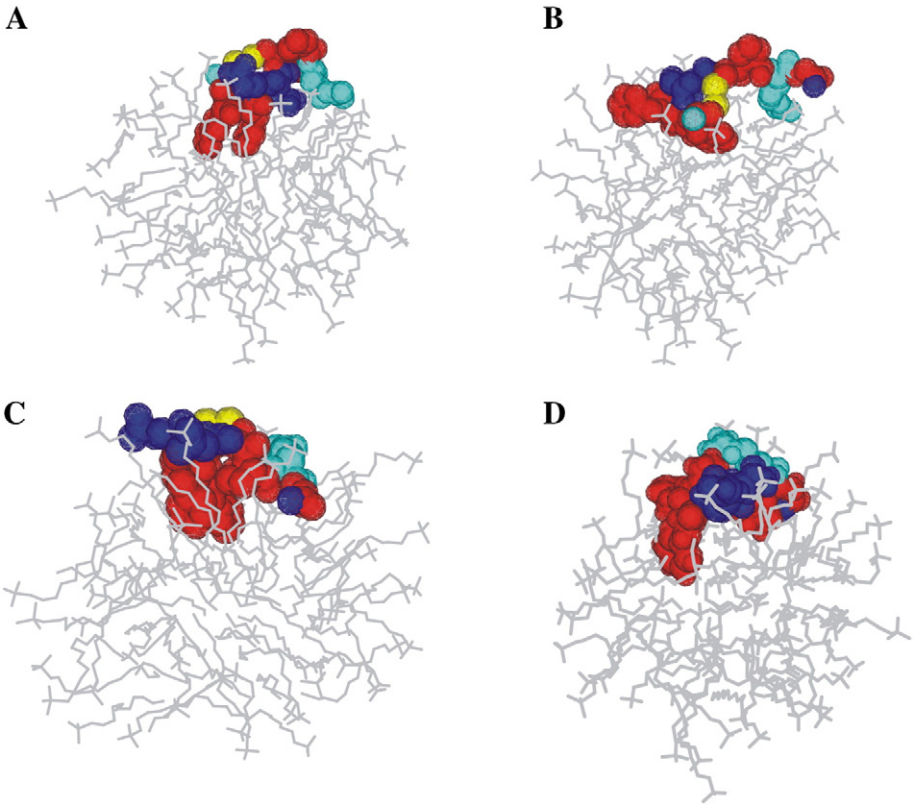

Fig. 5. The complexes of the structure with the highest statistical weight of (A) [L-Igl^2]AVP (**I**), (B) [D-Igl^2]AVP (**II**), (C) [Mpa^1,L-Igl^2]AVP (**III**) and (D) [Mpa^1,D-Igl^2]AVP (**IV**) with SDS micelle. The positively charged residues are displayed in cyan, the uncharged polar residue in blue, the hydrophobic residues in red. Additionally, the sulfur atoms are presented in yellow.

cyclic part. In addition, existence of the $d_{\alpha N}(2,4)$ connectivities in the NOESY spectra of analogs **II** and **IV** implies a β-turn at position 2,3 (numbers correspond to the two central residues of the β-turn). In the case of compound **IV**, the $d_{\alpha N}(1,4)$ NOE cross-peak found may also indicate β-turn at this position.

The $^3J_{HNH\alpha}$ coupling constants (Fig. 2) measured for the peptides are characteristic of either extended or unfolded states. Nevertheless, an averaging over at least two different conformations cannot be excluded. With analogs **I** and **III**, the $^3J_{HNH\alpha}$ coupling constants recorded for the L-Igl^2 and Phe^3 neighboring residues, (6.4 and 9.7; 7.4 and 9.7 for peptides **I** and **III**, respectively) suggest β-turn at position 2,3. This is the consequence of the steric hindrance imposed by the β-turn, which causes that the corner residues at positions $i+1$ and $i+2$ of the β-turn are characterized by low and high the $^3J_{HNH\alpha}$ coupling-constant values, respectively.

It is known that proline ϕ dihedral angle is relatively fixed at about −60°. The proline ring has also a significant effect on ψ dihedral angle resulting in two minima, −40° and 150° [45]. In turn, the high value of $^3J_{HNH\alpha}$ coupling constant for Arg^8 of analog **I** (10.2 Hz) corresponds to dihedral angle ϕ in the range of −140 to −100° [46,47]. Bearing all these facts in mind, we can expect one of the three types of β-turns, βI: $\phi_{i+1}=-60$, $\psi_{i+1}=-30$, $\phi_{i+2}=-90$, $\psi_{i+2}=0$, βII: $\phi_{i+1}=-60$, $\psi_{i+1}=120$, $\phi_{i+2}=80$, $\psi_{i+2}=0$ βVIII-turn ($\phi_{i+1}=-60$, $\psi_{i+1}=-30$, $\phi_{i+2}=-120$, $\psi_{i+2}=120$) [48] in the fragment Cys^6–Pro^7–Arg^8–Gly^9 of compound **I**.

The temperature coefficients of the amide protons (Fig. 2) of L-Igl^2, Arg^8 and Gly^9 of [L-Igl^2]AVP (**I**), D-Igl^2, Phe^3 and Gly^9 of [D-Igl^2]AVP (**II**), Arg^8 and Gly^9 of [Mpa^1,L-Igl^2]AVP (**III**) and Gln^4 of [Mpa^1,D-Igl^2]AVP (**IV**) were in the range of $-5<\Delta\delta/\Delta T<-3$ ppb/K, indicating weak intramolecular and/or solute–solvent hydrogen bonds. However, the shielding of the amide protons from solvent exchange might be dominated by interaction between the peptide and micelle, rather than by intramolecular interactions [49]. In the case of Gln^4 of compound **III**, the amide proton HN of Gln^4 is probably hydrogen bonding up to 30 °C, but it becomes broken at higher temperatures, which is manifested by higher tilt of temperature gradient in the range of 30–50 °C. Similar effect was observed for mesotocin in SDS/water solution [38].

The temperature coefficients of the remaining amide protons were more negative than −5 ppb/K, which rather excludes stable hydrogen bonds.

3.2. Conformational analysis of the calculated structures

The structures of the peptides are shown in Fig. 3 and are aligned to their mostly populated conformations using backbone atoms of the cyclic part of the molecules. The RMSD values for the ensemble of the structures are 0.288, 0.276, 0.226 and 0.195 Å for backbone atoms of cyclic part of analogs **I**, **II**, **III** and **IV**, respectively.

The common conformational feature (Table 1) of all the analogs is a β-turn at position 2,3. In the analogs **I** and **III**, this β-turn is stabilized by the HN^4–CO^1 hydrogen bond. In turn, in the case of analogs **II** and **IV**, the β-turn at position 2,3 is not tight enough and the Gln^4 HN amide proton is not hydrogen bonding. Three of the analogs, namely **II**, **III** and **IV** create additional β-turn at position 3,4. Nevertheless, this β-turn is distorted. Therefore, their existence may not result directly from NMR data.

The analog **III**, as the only one, adopts a β-turn at position 4,5. This β-turn is not closed by hydrogen bond, which is a consequence of distortion of either the ψ_4 or ϕ_5 dihedral angles. In addition, an inverse γ-turn over the Pro^7 was found for compound **III**. In turn, the C-terminus of the peptide **I** is involved in a β-turn in the Cys^6–Gly^9 fragment. While simultaneously, it assumes a hydrogen-bonded βI- or βIII-turn at position 6,7.

The averaged radii of gyration (Rg) (Table 1) calculated with all of the heavy atoms for each analog indicate that the conformation of the

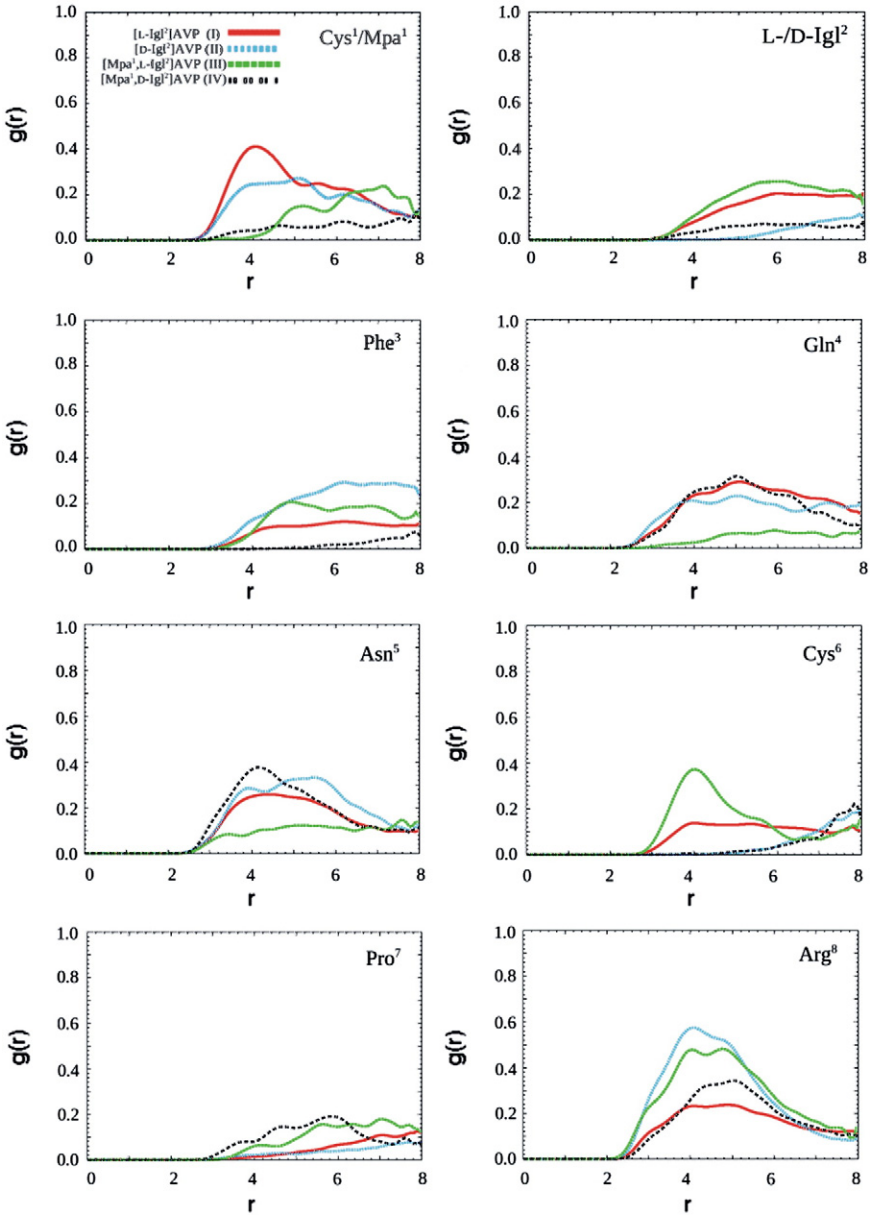

Fig. 6. Radial distribution functions g(r) between the sulfate head groups on SDS micelle and the side chain (heavy atoms) of each residue. The r parameter defines the distance in Å.

analog **II** is noticeably more extended than the remaining analogs, this being due to a more outstretched structure of the acyclic part of the molecule. The differences in the Rg values obtained for the cyclic part of each analog are comparable, indicating similar sizes of the tocin rings.

3.3. Conformation of the aromatic side chains

All the structures were submitted to statistical study of relative orientation of the Igl/D-Igl[2] and Phe[3] aromatic side chains. It is clearly seen (Fig. 4A) that the preferred rotamer about the χ_1 torsion angle of Igl is gauche(−) for both analogs with L-Igl, **I** and **III**, and either trans or gauche(+) for **II** and **IV**, respectively. A relationship has been established between the flat angle between the planes of aromatic rings ($F_{\text{Igl-Phe}}$) and a dihedral angle between two planes, where the former is determined by the mass centre of aromatic part of Igl/D-Igl[2], Cα of Igl/D-Igl[2] and Cα of Phe[3], whereas the latter by Cα of Igl/D-Igl[2], Cα of Phe[3] and the centre of mass of aromatic ring of Phe[3] ($D_{\text{Igl-Phe}}$) (Fig. 4B). Taking into account the flat angle, $F_{\text{Igl-Phe}}$, the structure of all the peptides, with the exception of analog **IV**, can be divided into two groups based on different orientation of the Phe[3] side chain caused by changes of its χ_2 dihedral angle (Fig. 4A). In turn, the dihedral angle values, $D_{\text{Igl-Phe}}$, are clustered about horizontal lines, one for each peptide, $D_{\text{Igl-Phe}} = 15°$, 85°, 13° and 65° for analogs **I**, **II**, **III** and **IV**, respectively, where the angles correspond to average values of $D_{\text{Igl-Phe}}$. As seen, the $D_{\text{Igl-Phe}}$ values are noticeably greater for analogs modified with the D enantiomer of Igl. The differences in the $D_{\text{Igl-Phe}}$ values are most of all the consequence of the change of Igl configuration from L to D, which evidently alters the side chain orientation.

3.4. Radial distribution functions and hydration numbers for the AVP analogs in SDS micelle

During molecular dynamics simulations, the peptides diffused from the hydrophobic core of the SDS micelle to the interface to adopt energetically more favorable conformation. The position of the peptides on the micellar surface becomes fixed after ca. 2 ns of MD. Thereafter, the peptides remain bound to the interface for a further 4 ns of LES simulations. Fig. 5 presents the structures of the peptides with the highest statistical weight binding with the SDS micelle. The

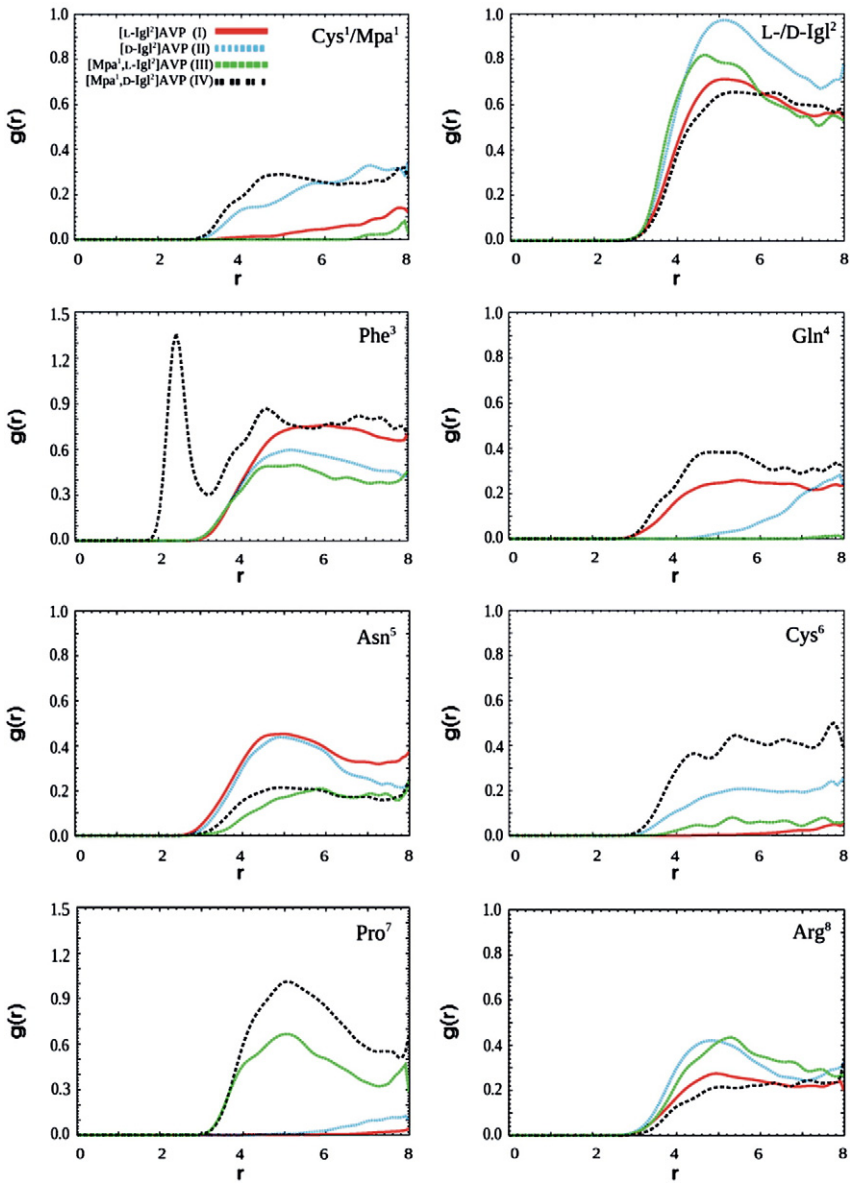

Fig. 7. Radial distribution functions g(r) between the micelle core and the side chain (heavy atoms) of each residue. The r parameter defines the distance in Å. Note different scale for residues 3 and 7.

peptide–micelle interactions were analyzed by the radial distribution function (RDF) values for all the amino acids in each peptide (Figs. 6 and 7). In addition, the hydration numbers were calculated to investigate interaction with water molecules (Table 2).

In each peptide the aromatic residues, Igl/D-Igl[2] and Phe[3] are deeply immersed into the hydrophobic micelle core as additionally confirmed by low hydration numbers calculated for their side chains. Nevertheless, the backbone oxygen atoms of both D-Igl[2] and Phe[3] in compound **IV** are strongly hydrated in contrast to the remaining peptides.

The positively charged centre on the Arg side chain shows the tendency to be associated with sulfate ions of SDS and at the same time, it is located near the hydrophobic part of the micelle. In turn, the oxygen atom of Arg[8] is exposed to the aqueous environment in each case. The analogs **I** and **II** possess also the positively charged N-terminus, and consequently the stronger interactions between the N-terminus and negatively charged sulfate head groups of the SDS micelle is noticed than for the deamino analogs (Fig. 6). In turn, in the deamino analogs, **III** and **IV**, the Pro[7] side chain clearly penetrates interior of the SDS micelle (Fig. 7). Moreover, the hydration numbers (Table 2) indicate that also the oxygen atom of Pro is embedded into the hydrophobic micelle core. The common feature of the deamino analogs are also high hydration number calculated for a backbone oxygen atom of Gln[4], which indicates that it is exposed to the aqueous phase. In the case of peptide **III**, the Gln[4] side chain is also characterized by a high hydration number.

The side chains of residues 1 and 6 of the D-Igl-modified analogs, **II** and **IV**, are evidently more deeply embedded into the micelle core than in the remaining ones and consequently disulfide bridges of both peptides are hidden from the aqueous phase.

3.5. Biological relevance of the modifications

It becomes clear that all the analogs exhibit the tendency to adopt β-turns at positions 2,3 and/or 3,4, which is characteristic of oxytocin-like peptides [50]. Thus, the high affinity of the analogs to the OT receptors might be due to these reverse structures. Moreover, it seems likely that the strong π–π interactions between aromatic side chains of the vasopressin-like peptides and the aromatic residue cluster, located in TM6 OT and V_{1a} receptor, might be responsible for antagonistic properties [51]. It is also known that the amino acid at position 2 of a ligand plays a key role in the antagonistic effect. Insertion of a bulky

Table 2
Hydration numbers for each residue of [Igl^2]AVP (**I**), [D-Igl^2]AVP (**II**), [Mpa^1,Igl^2]AVP (**III**) and [Mpa^1,D-Igl^2]AVP (**IV**) in SDS micelle/water system. The hydration numbers were averaged over the conformations with significant weights—comprising 60% of the ensemble for each analog.

Residue	Carbonyl oxygen				Side chains			
	I	II	III	IV	I	II	III	IV
Cys^1/Mpa^1	0.21	0.15	0.55	0.15	0.34	0.21	0.30	0.16
L-Igl^2/D-Igl^2	0.09	0.00	0.02	0.40	0.05	0.01	0.01	0.05
Phe^3	0.20	0.35	0.21	0.57	0.01	0.15	0.01	0.00
Gln^4	0.36	0.19	0.56	0.64	0.27	0.25	0.48	0.17
Asn^5	0.01	0.56	0.59	0.0	0.08	0.35	0.28	0.33
Cys^6	0.55	0.32	0.33	0.21	0.33	0.20	0.27	0.02
Pro^7	0.78	0.57	0.12	0.00	0.24	0.31	0.00	0.00
Arg^8	0.55	0.77	0.47	0.47	0.28	0.20	0.20	0.28
Gly^9	0.61	0.88	0.81	0.58	–	–	–	–

lipophilic D-amino acid at this position enhances often antioxytocic properties [14], and at the same time alters the side chain orientation. Consequently, mutual arrangement of the side chains of neighboring residues at positions 2 and 3 undergoes changes. A closer examination of the indanylglycine χ_1 space angle suggests that the common feature of analogs **I** and **III** is the gauche(−) conformation of the Igl side chain, which may be crucial for selectivity in this series of analogs, given that both analogs exhibit only antiuterotonic activity. On the other hand, a comparison of the flat $F_{\text{Igl-Phe}}$ and dihedral $D_{\text{Igl-Phe}}$ angles (see Conformation of the aromatic side chains section) of the analogs has shown that the latter adopts greater values for analogs **II** and **IV**, which are blockers of both the OT and V_{1a} receptors. A similar tendency was reported for AVP analogs modified with N-methylpenylalanine enantiomers at positions 2 and 3 [52].

Earlier investigations have shown that replacement of Gln^4 in AVP reduced significantly the affinity toward V_{1a} receptors [53,54]. Moreover, the hydrogen bond between the Thr$^{7.38}$333 hydroxyl of V_{1a} receptor and the carboxamide of the AVP Gln^4 was found to be important for AVP binding [55]. In addition, Thr$^{7.38}$333 was proposed as the residue controlling the V_{1a}/V_2 binding selectivity for vasopressin antagonists [56]. Hence, the orientation of Gln^4 side chain of a ligand seems to be important for V_{1a} receptor affinity. In each of the peptides studied, the Gln^4 side chain is folded back over the ring moiety. However, it lies on the opposite face of the tocin moiety in analogs with L and D enantiomers of Igl, which can additionally explain their different activities towards the V_{1a} receptor.

4. Conclusions

The affinity of the vasopressin analogs to respective receptors is a consequence of their structure and conformation. For this reason, a correlation between the structure and conformation can provide valuable data to design new analogs with appropriate biological activity. However, short peptides, such as vasopressin, usually adopt unstable conformation and exist in many conformations at equilibrium. Multiple conformations occurring in a dynamic exchange produce averaged NMR parameters, which hamper unequivocal conformational analysis. Hence, all the available NMR data should be examined with caution.

The primary purpose of substitution of indanylglycine (Igl) at position 2 of the AVP analogs was to reduce their flexibility and to change pharmacological profile of the peptides. Moreover, using the SDS micelle in the NMR studies may additionally restrict conformational freedom of the peptides and probably induces a conformation, which is supposed to be bound to the receptor.

In summary, the new AVP analogs should be designed in such a way, as to preserve specific conformation of a peptide and the proper mutual arrangement of the side chains. Moreover, it should be remembered that the structurally restricted modifications reduce the flexibility of a peptide thus enabling a more precise conformational analysis to be made. Introduction of a D-amino acid in the second position of the AVP analogs changes the side chain orientation and enforces the possibility of β-turn formation in a 1–4 fragment, which is characteristic of oxytocin-like peptides. Furthermore, the specific orientation of the side chains at positions 2 and 3 is important for antagonistic properties. In addition, the Gln^4 side chain arrangement seems to be crucial for V_{1a} receptor affinity.

Acknowledgements

This work was supported by Polish State Committee for Scientific Research under the grant No. N N204 181736 and DS 8360-4-01330-0. The calculations were carried out in the Academic Computer Centre (TASK) in Gdańsk, Poland.

Appendix A. Supplementary data

Supplementary data associated with this article can be found, in the online version, at doi:10.1016/j.bpc.2010.06.002.

References

[1] M. Barlow, Vasopressin, Test Emerg. Med. 14 (2002) 304–314.
[2] M. Birnbaumer, Vasopressin receptors, Trends Endocrinol. Metab. 11 (2000) 406–410.
[3] S. Jard, R.C. Gaillard, G. Guillon, J. Marie, P. Schoenenberg, A.F. Muller, M. Manning, W.H. Sawyer, Vasopressin antagonists allow demonstration of a novel type of vasopressin receptor in the rat adenohypophysis, Mol. Pharmacol. 30 (1986) 171–177.
[4] Z. Wang, L.J. Young, G.J. De Vries, T.R. Insel, Voles and vasopressin: a review of molecular, cellular and behavioral studies of pair bonding and paternal behaviors, Prog. Brain Res. 119 (1998) 483–499.
[5] C. Barberis, B. Mouillac, T. Durroux, Structural bases of vasopressin/oxytocin receptor function, J. Endocrinol. 156 (1998) 223–229.
[6] C.J. Newschaffer, L.A. Croen, J. Daniels, E. Giarelli, J.K. Grether, S.E. Levy, D.S. Mandell, L.A. Miller, J. Pinto-Martin, J. Reaven, A.M. Reynolds, C.E. Rice, D. Schendel, G.C. Windham, The epidemiology of autism spectrum disrorders, Annu. Rev. Public Health 28 (2007) 235–258.
[7] T.R. Insel, D.J. O'Brien, J.F. Leckman, Oxytocin, vasopressin, and autism: is there a connection? Biol. Psychiatry 45 (1999) 145–157.
[8] K. Palczewski, T. Kumasaka, T. Hori, C.A. Behnke, H. Motoshima, B.A. Fox, I. Le Trong, D.C. Teller, T. Okada, R.E. Stenkamp, M. Yamamoto, M. Miyamoto, Crystal structure of rhodopsin: a G protein-coupled receptor, Science 289 (2000) 739–745.
[9] R.J. Schwayzer, In search of the 'bio-active conformation'—is it induced by the target cell membrane? Mol. Recog. 8 (1995) 3–8.
[10] D.F. Mierke, C. Giragossian, Peptide hormone binding to G-protein-coupled receptors: structural characterization via NMR techniques, Med. Res. Rev. 21 (2001) 450–471.
[11] J. Hlavacek, Important Structural Modifications. Noncoded Amino Acid, in: K. Jošt, M. Lebl, F. Brtnik (Eds.), Handbook of Neurohypophyseal Hormone Analogs, Part 2, vol. 1, CRC Press Inc., Boca Raton, Florida, 1987, pp. 109–129.
[12] V.J. Hruby, M.S. Chow, D.D. Smith, Conformational and structural considerations in oxytocin-receptor binding and biological activity, Annu. Rev. Pharmacol. Toxicol. 30 (1990) 501–534.
[13] K. Bakos, J. Havass, F. Fülöp, L. Gera, J.M. Stewart, G. Falkay, G.K. Tóth, Synthesis and receptor binding of oxytocin analogs containing conformationally restricted amino acids, Lett. Pept. Sci. 8 (2002) 35–40.
[14] B. Jójárt, Á. Márki, Comparative study of eight oxytocin antagonists by simulated annealing, J. Mol. Model. 12 (2006) 823–828.
[15] R. Sankararamakrishnan, Recognition of GPCRs by peptide ligands and membrane compartments theory: structural studies of endogenous peptide hormones in membrane environment, Biosci. Rep. 26 (2006) 131–158.
[16] L. Gera, J.M. Stewart, A new class of bradykinin antagonists containing indanylglycine, Immunopharmacology 33 (1996) 174–177.
[17] W.H. Sawyer, M. Acosta, M. Manning, Structural changes in the arginine vasopressin molecule that prolong its antidiuretic action, Endocrinology 95 (1974) 140–149.
[18] Z. Grzonka, F. Kasprzykowski, L. Lubkowska, K. Darlak, T.A. Hahn, A.F. Spatola, In vitro degradation of some arginine-vasopressin analogs by homogenates of rat kidney, liver, and serum, Pept. Res. 4 (1991) 270–274.
[19] A. Kwiatkowska, M. Ślęszyńska, I. Derdowska, A. Prahl, D. Sobolewski, L. Borovickova, J. Slaninowa, B. Lamek, Novel analogues of arginine vasopressin containing α-2-indanylglycine enantiomers in position 2, J. Pept. Sci. 16 (2010) 15–20.
[20] C. Cosola, M. Albrizio, A.C. Guaricci, M.A. De Salvia, A. Zarrilli, R.L. Sciorsci, R. Minoia, Opioid agonist/antagonist effect of naloxone in modulating rabbit jejunum contractility *in vitro*, J. Physiol. Pharm. 57 (2006) 439–449.
[21] A. Bax, R. Freeman, Enhanced NMR resolution by restricting the effective sample volume, J. Magn. Reson. 65 (1985) 355–360.

[22] M. Rance, O.W. Sorenson, G. Bodenhausen, G. Wagner, R.R. Ernst, K. Wüthrich, Improved spectral resolution in cosy ^{1}H NMR spectra of proteins via double quantum filtering, Biochem. Biophys. Res. Commun. 117 (1983) 479–485.
[23] A. Kumar, R.R. Ernst, K. Wüthrich, A two-dimensional nuclear Overhauser enhancement (2D NOE) experiment for the elucidation of complete proton–proton cross relaxation networks in biological macromolecules, Biochim. Biophys. Res. Commun. 95 (1980) 1–10.
[24] A.A. Bothner-By, R.L. Stephens, J.M. Lee, C.D. Warren, R.W. Jeanloz, Structure determination of a tetrasaccharide: transient nuclear Overhauser effects in the rotating frame, JACS 106 (1980) 811–813.
[25] A. Bax, D.G. Davis, Practical aspects of two-dimensional transverse NOE spectroscopy, J. Magn. Reson. 63 (1985) 207–213.
[26] A.G. Palmer, J. Cavanagh, P.E. Wright, M. Rance, Sensitivity improvement in proton-detected two-dimensional heteronuclear correlation spectroscopy, J. Magn. Reson. 93 (1991) 151–170.
[27] L.E. Kay, P. Keifer, T. Saarinen, Pure absorption gradient enhanced heteronuclear single quantum correlation spectroscopy with improved sensitivity, JACS 114 (1992) 10663–10665.
[28] J. Schleucher, M. Schwendinger, M. Sattler, P. Schmidt, O. Schedletzky, S.J. Glaser, O.W. Sorensen, C. Griesinger, A general enhancement scheme in heteronuclear multidimensional NMR employing pulsed field gradients, J. Biomol. NMR 4 (1994) 301–306.
[29] D.S. Wishart, C.G. Bigam, A. Holm, R.S. Hodges, B.D. Sykes, 1H, 13C and 15N random coil NMR chemical shifts of the common amino acids. I. Investigations of nearest-neighbor effects, J. Biomol. NMR 5 (1995) 67–81.
[30] C. Bartles, T. Xia, M. Billeter, P. Günter, K. Wüthrich, The program XEASY for the computer-supported NMR spectral analysis of biological macromolecules, J. Biomol. NMR 5 (1995) 1–10.
[31] M. Groth, J. Malicka, C. Czaplewski, S. Ołdziej, L. Łankiewicz, W. Wiczk, A. Liwo, Maximum entropy approach to the determination of solution conformation of flexible polypeptides by global conformational analysis and NMR spectroscopy—application to DNS1-c-[D-A2bu2, Trp4, Leu5]-enkephalin and DNS1-c-[d-A2bu2, Trp4, D-Leu5]enkephalin, J. Biomol. NMR 15 (1999) 315–330.
[32] D.A. Case, T.A. Darden, T.E. Cheatham III, C.L. Simmerling, J. Wang, R.E. Duke, R. Luo, K.M. Merz, D.A. Pearlman, M. Crowley, R.C. Walker, W. Zhang, B. Wang, S. Hayik, A. Roitberg, G. Seabra, K.F. Wong, F. Paesani, X. Wu, S. Brozell, V. Tsui, H. Gohlke, L. Yang, C. Tan, J. Mongan, V. Hornak, G. Cui, P. Beroza, D.H. Mathews, C. Schafmeister, W.S. Ross, P.A. Kollman, AMBER 9, University of California, San Francisco, 2006.
[33] F.H. Allen, W.D.S. Motherwell, Applications of the Cambridge Structural Database in organic chemistry and crystal chemistry, Acta Cryst. B58 (2002) 407–422.
[34] M.W. Schmidt, K.K. Baldridge, J.A. Boatz, S.T. Elbert, M.S. Gordon, J.H. Jensen, S. Koseki, N. Matsunaga, K.A. Nguyen, S. Su, T.L. Windus, M. Dupuis, J.A. Montgomery, General atomic and molecular electronic structure system, J. Comput. Chem. 14 (1993) 1347–1363.
[35] C.I. Bayly, P. Cieplak, W.D. Cornell, P.A. Kollman, A well-behaved electrostatic potential based method using charge restraints for deriving atomic charges: the RESP model, J. Phys. Chem. 97 (1993) 10269–10280.
[36] K.J. Schweighofer, U. Essman, M. Berkowitz, Simulation of sodium dodecyl sulfate at the water-vapor and water-carbon tetrachloride interfaces at low surface coverage, J. Phys. Chem. B 101 (1997) 3793–3799.
[37] C.D. Bruce, M.L. Berkowitz, L. Perera, M.D.E. Forbes, Molecular dynamics simulation of sodium dodecyl sulfate micelle in water: micellar structural characteristics and counterion distribution, J. Phys. Chem. B 106 (2002) 3788–3793.
[38] S. Rodziewicz-Motowidło, E. Sikorska, M. Oleszczuk, C. Czaplewski, Conformational studies of vasopressin and mesotocin using NMR spectroscopy and molecular modeling methods. Part II: studies in the SDS micelle, J. Pept. Sci. 14 (2008) 85–96.
[39] X. Cheng, V. Hornak, C. Simmerling, Improved conformational sampling through an efficient combination of mean-field simulation approaches, J. Phys. Chem. B 108 (2004) 426–437.
[40] R. Meadows, C.B. Post, B.A. Luxon, D.G. Gorenstein, MORASS 2.1 Program, Purdue University, W. Lafayette, , 1994.
[41] V.F. Bystrov, Spin–spin coupling and the conformational states of peptide system, Progr. NMR Spectrosc. 10 (1976) 41–81.
[42] C. Yu, T.H. Yang, C.J. Yeh, L.C. Chuang, Combined use of NMR, distance geometry, and retrained energy minimization for the conformational analysis of 8-lysinevasopressin, Can. J. Chem. 70 (1992) 1950–1955.
[43] R. Koradi, M. Billeter, K. Wüthrich, MOLMOL: a program for display and analysis of macromolecular structures, J. Mol. Graph. 14 (1996) 52–55.
[44] H.J. Dyson, M. Rance, R.A. Houghten, R.A. Lerner, P.E. Wright, Folding of immunogenic peptide fragments of proteins in water solution. I Sequence requirements for the formation of a reverse turn, J. Mol. Biol. 201 (1988) 161–200.
[45] M.P. Wiliamson, The structure and function of proline-rich regions in proteins, Biochem. J. 297 (1994) 249–260.
[46] A. Pardi, M. Billeter, K. Wüthrich, Calibration of the angular-dependence of the amide proton-C-alpha proton coupling-constants, $^{3}J_{HNH\alpha}$, in a globular protein—use of $^{3}J_{HNH\alpha}$ for identification of helical secondary structure, J. Mol. Biol. 180 (1984) 741–751.
[47] M. Eberstadt, G. Gemmecker, D.F. Mierke, H. Kessler, Scalar coupling constants—their analysis and their application for the elucidation of structures, Angew. Hem. Int. Ed. Engl. 34 (1995) 1671–1695.
[48] P.N. Lewis, F.A. Momany, H.A. Scheraga, Chain reversals in proteins, Biochim. Biophys. Acta 303 (1973) 211–229.
[49] S. De Luca, R. Ragone, C. Bracco, G. Digilio, L. Aloj, D. Tesauro, M. Saviano, C. Pedone, G. Morelli, A cyclic CCK8 analogue selective for the cholecystokin type A receptor: design, synthesis, NMR structure and binding measurements, Chembiochem 4 (2003) 1176–1187.
[50] A. Liwo, A. Tempczyk, S. Ołdziej, M.D. Shenderovich, V.J. Hruby, S. Talluri, J. Ciarkowski, F. Kasprzykowski, L. Łankiewicz, Z. Grzonka, Exploration of the conformational space of oxytocin and arginine-vasopressin using the electrostatically driven Monte Carlo and molecular dynamics methods, Biopolymers 38 (1996) 157–175.
[51] M.J. Ślusarz, E. Sikorska, R. Ślusarz, J. Ciarkowski, Molecular docking-based study of vasopressin analogues modified at positions 2 and 3 with N-methylphenylalanine: influence on receptor-bound conformations and interactions with vasopressin and oxytocin receptors, J. Med. Chem. 49 (2006) 2463–2469.
[52] E. Sikorska, M.J. Ślusarz, B. Lammek, Conformational studies of vasopressin analogues modified with N-methylphenylalanine enantiomers in dimethyl sulfoxide solution, Biopolymers 82 (2006) 603–614.
[53] W.H. Sawyer, M. Acosta, L. Balaspiri, J. Judd, M. Manning, Structural changes in the arginine vasopressin molecule that enhance antidiuretic activity and specificity, Endocrinology 94 (1974) 1106–1115.
[54] D. Gillessen, V. du Vigneaud, The synthesis and pharmacological properties of 4-decarboxamide-8-1ysinevasopressin, 5-decarboxamide-8-1ysinevasopressin, and their l-deamino analogs, J. Biol. Chem. 242 (1967) 4806–4812.
[55] M.J. Ślusarz, A. Giełdoń, R. Ślusarz, J. Ciarkowski, Analysis of interactions responsible for vasopressin binding to human neurohyphophyseal hormone receptors—molecular dynamics study of the activated receptor-vasopressin-Gα systems, J. Pept. Sci. 12 (2006) 180–189.
[56] N. Cotte, M.N. Balestre, A. Aumelas, E. Mahé, S. Phalipou, D. Morin, M. Hibert, M. Manning, T. Durroux, C. Barberis, B. Mouillac, Conserved aromatic residues in the transmembrane region VI of the V1a vasopressin receptor differentiate agonist vs. antagonist ligand binding, Eur. J. Biochem. 267 (2000) 4253–4263.